

***Ab-Initio* and Conformational Analysis of a Potent VEGFR-2 Inhibitor: A Case Study on Motesanib**

Ahmad Ebadi^{a,b}, Nima Razzaghi-Asl^c, Sara Shahabipour^a and Ramin Miri^{a,b*}

^aMedicinal and Natural Products Chemistry Research Center, Shiraz University of Medical Sciences, Shiraz, Iran. ^bDepartment of Medicinal Chemistry, School of Pharmacy, Shiraz University of Medical Sciences, Shiraz, Iran. ^cDepartment of Medicinal Chemistry, School of Pharmacy, Ardabil University of Medical Sciences.

Abstract

Vascular endothelial growth factor receptor-2 (VEGFR-2); a cell surface receptor for vascular endothelial growth factors, is a key pharmacological target involved in the cell proliferation/angiogenesis. It has been revealed that VEGFR-2 induces proliferation through activation of the extracellular signal-regulated kinases pathway. In this regard, targeting the VEGFR-2 has been considered as an efficient route to develop anti-tumor agents. Motesanib is a small-molecule antagonist of VEGFR-1, 2, and 3 (IC₅₀s; 2 nM, 3 nM, 6 nM, respectively). It is an experimental drug candidate undergoing clinical trials against some types of cancer. In the present study, Motesanib (AMG 706) was evaluated in terms of its binding energies with individual amino acids of VEGFR-2 active site (amino acid decomposition analysis). For this purpose, functional B3LYP associated with split valence basis set using polarization functions (Def2-SVP) was used. Comparative conformational analysis of the ligand in optimized and crystallographic states revealed that Motesanib does not necessarily bind to the VEGFR-2 active site in its minimum energy conformer.

Keywords: VEGFR-2; Motesanib; Cancer; B3LYP; DFT.

Introduction

Vascular endothelial growth factors (VEGFs) bind to three structurally related receptor tyrosine kinases; VEGFR-1, VEGFR-2, and VEGFR-3. A number of coreceptors such as neuropilins that lack intrinsic catalytic activity bind to VEGF and also modulate the effect of the VEGFRs (1). VEGFRs have a high degree of homology within the kinase domain; however, their signaling properties greatly differ (1). VEGFR-2 is the major mediator of responses in endothelial cells and it is considered to be a

principal signal transducer in angiogenesis (2). Vascular endothelial growth factor receptor 2 (VEGFR-2) is a cell surface receptor for VEGFs (3, 4). VEGF signaling pathway has been well demonstrated to induce angiogenesis during tumor development (5, 3). Vascular endothelial growth factor (VEGF) has been found to be a major driver of tumor angiogenesis leading to efforts in development of novel therapeutics aimed at inhibiting its activity. It is generally accepted that the destructive growth of tumors and their metastases is highly depended on angiogenesis (6).

Anti-VEGF therapy has been regarded as a prominent choice for the management of several human malignancies. The vast majority of solid

* Corresponding author:
E-mail: mirir@sums.ac.ir

tumors are involved with VEGF overexpression (7). In this regard, chemical agents with the inhibitory activity on angiogenesis may be focused as a workable treatment options for patients involved with solid tumors (8). Inhibition of VEGF has been reported to significantly suppress tumor angiogenesis in mouse tumor models (9). The angiogenesis process of solid tumors may be avoided due to the inhibition of the tyrosine kinase VEGFR-2 signaling pathway. In this way required blood flow for developing tumor would decrease dramatically and even the growth will stopped because of lack of nutrient and growth factors supported by freshly forming vessels (10,11). Hence, anti-tumor drug development targeting VEGFR-2 signalling pathway has been recently highlighted as an important way in the clinical trials (12).

A number of structurally diverse small molecule VEGFR-2 inhibitors such as indolin-2-ones, phthalazines, quinolinones, imidazopyridines, benzimidazoles, quinoline amides, pyridines and quinazolines have been introduced in the literature (13-19). In a typical lead/drug discovery protocol, potential candidate molecules may suffer from undesirable properties in their pharmacokinetic and pharmacodynamic profiles. Structure-based drug design has been considered as one of the major strategies in achieving potential drug candidates (20,21). Motesanib (N-(3,3-dimethyl-2,3-dihydro-1H-indol-6-yl)-2-((pyridin-4-ylmethyl)amino)pyridine-3-carboxamide) is an experimental drug candidate which has been exhibited antagonistic activity for VEGFR-2 (22). Clinical trials on potential beneficial effects of Motesanib against some types of cancers are being actively pursued. Results showed that Motesanib inhibited VEGFR-1, 2, and 3 with IC₅₀ values of 2, 3 and 6 nM respectively (23-25).

In lead-drug development strategies, combination of experimental methods with computer aided molecular design (CAMD) techniques is essential for the development of new drugs aimed at new targets, and thus for medicinal chemistry (26). Various computational chemistry methods are in hand for running CAMD. These methods

comprise mainly two categories; ligand-based and structure-based methods. Within this scenario, theoretical methods based on density- functional theory (DFT) are going to play an increasingly important role in many applications of computational chemistry to drug discovery (27-29). One of the mostly used DFT methods is Becke three-parameter Lee-Yang-Parr (B3LYP) hybrid density functional theory (30). This technique has been applied for conformational analysis of antiangiogenic agents such as Motesanib (31). Estimating the proportion of individual amino acid-ligand interaction energies in total binding energy would be a very useful trend in pharmacophore discernment and development (Amino acid decomposition analysis). No such report could be found for Motesanib with VEGFR-2.

In continuation to our interest in developing new cytotoxic agents (32), we aimed to determine the binding pose and binding energies of Motesanib in VEGFR-2 active site. For this purpose, DFT calculations at the level of B3LYP/Def2-SVP were used to estimate the individual amino acid-ligand interaction energies. Furthermore; conformational analysis of Motesanib was performed at the same level of theory to determine the torsional deviation from minimum energy state upon binding to the receptor.

Experimental

Computational section

X-ray crystallographic structure of VEGFR-2 with its cognate ligand (AMG 706) was downloaded from Brook Haven Protein databank (PDB code: 3EFL, www.rcsb.org). All the pre-processing procedure for ligand and receptor crystallographic files were done within WHAT IF server (European Molecular Laboratory Heidelberg, Germany). All hydrogens were properly added to the receptor PDB file using What if server. All computational DFT studies were performed using functional B3LYP associated with split valence basis set using polarization functions (Def2-SVP) (33).

The evaluated amino acid residues in *ab initio* study (Leu889, Ala866, Lys868, Glu885, Val899, Val916, Cys919, Leu1035, Asp1046)

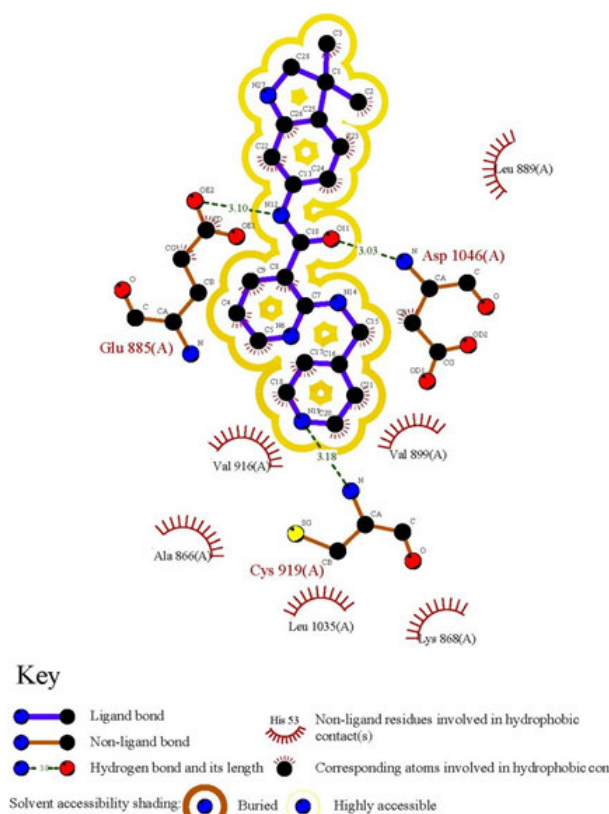


Figure 1. 2D representation of ligand-receptor interactions for Motesanib in VEGFR-2 active site.

were chosen according to the information from crystallographic data (34). The proposed interaction profile could be found in Brook Haven Protein databank. All amino acids were considered in their real electrostatic state. For each residue under study, N-terminal was acetylated and C-terminal was methyl amidated to mimic the original electron density. All conformational and configurational features were the same as the X-ray structure. However the positions of hydrogen bonds are not clearly recognized in a typical X-ray crystallographic file and this restriction persuaded us to further optimize the heavy atom-hydrogen bonds using constrained optimization method (heavy atom fixing approximation).

All ligand-receptor interaction energies were estimated by B3LYP/ Def2-SVP method. The whole calculations were done with the ORCA quantum chemistry package (30). The optimized structures were visualized by Visual Molecular Dynamics program (VMD) (35).

Results and Discussion

Ab initio study of ligand-receptor interactions

To obtain a binding profile between a Motesanib and VEGFR-2 active site, relevant amino acids were chosen on the basis of information from Protein Data Bank (PDB). The representation of the Motesanib structure in the active site of VEGFR-2 was further confirmed via schematic 2D interaction profile generated by LIGPLOT Figure 1.

The directionality of hydrogen bonds including optimum distances and angles supports efficient interactions with receptor. Bearing this in mind, the optimization process was done with the same basis set to obtain the exact geometry of H-bonds. The related data are summarized in Table 1. Hydrogen bond geometries were described as H-donor-acceptor angles. It should be noted that hydrogen bond lengths were obtained considering H-acceptor distances.

Ligand-residue binding energies (ΔE_b) were

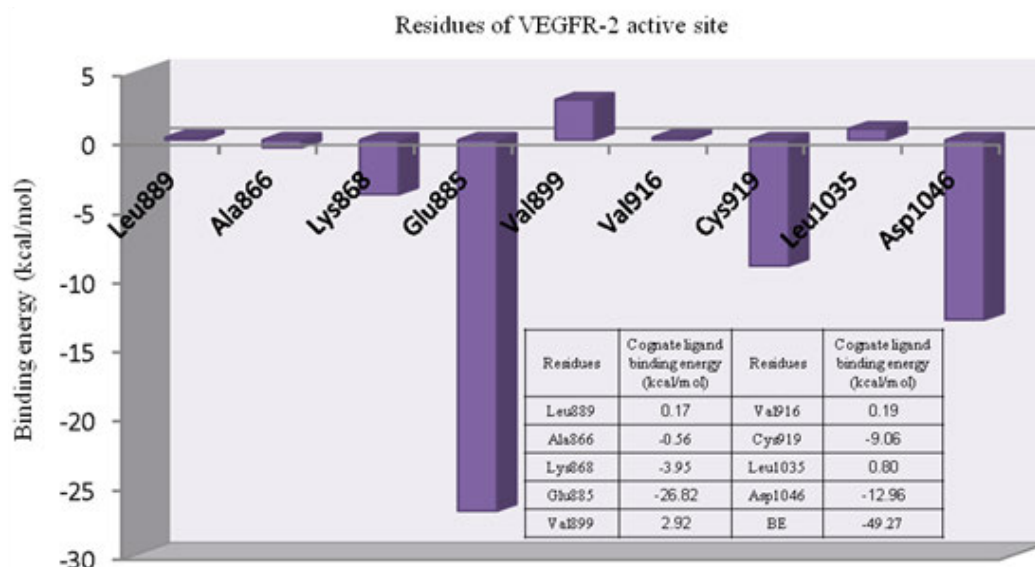


Figure 2. Individual residue-ligand interaction energies for Motesanib and VEGFR-2.

calculated using the following equation:

$$\Delta E_b = E_{LR} - E_L - E_R \quad \text{Equation (1)}$$

E_{LR} stands for residue-ligand interaction energy, E_R and E_L indicate the electronic energies for residues and ligand, respectively. Individual ligand-residue binding energies are shown in Figure 2.

Lipophilic contacts are a function of orientation, constant/induced dipole moments and distance (36). Attractive hydrophobic interaction was made between AMG 706 and Ala866 residue (-0.56 cal/mol). Regarding the obtained results, one may assume that electrostatic hydrogen bonding interactions may have significant contribution to total binding energy between AMG 709 and receptor. For Leu889, Val899, Val916 and Leu1035 the positive binding energies might be related to an inappropriate orientation of ligand in the active site of receptor (crystallographic state). It

should be noticed that molecular dynamic may assist in balancing these close contacts which are responsible for repulsive interactions with receptor.

The role of cation- π interaction as a force for molecular recognition in biological media has been revealed via studies on model systems and the analysis of biological macromolecular structures (36). In Lys868 the quaternary amine moiety might be responsible for observed cation- π interaction with central pyridine ring of AMG 709 (-3.93 kcal/mol). Binding pose of the ligand revealed that nitrogenous cation centered on the top of the π face of pyridine ring (Figure 3). Our estimated energy for the associated cation- π interaction correlated well with previously reported data (37), but might be less than accepted values (38). This energy difference might be attributed to the existence of pyridine lone pair. In pyridine, the lone pair does not participate in aromaticity and thus electronegativity of the heteroatom wins out and

Table 1. Hydrogen-bond analysis of cognate inhibitor (Motesanib) with VEGFR-2 residues.

Amino acid	Optimized hydrogen bond distances (Å) state	hydrogen bond angle (degree)
Glu885	2.11	11.66
Asp1046	2.04	9.60
Cys919	2.19	5.21

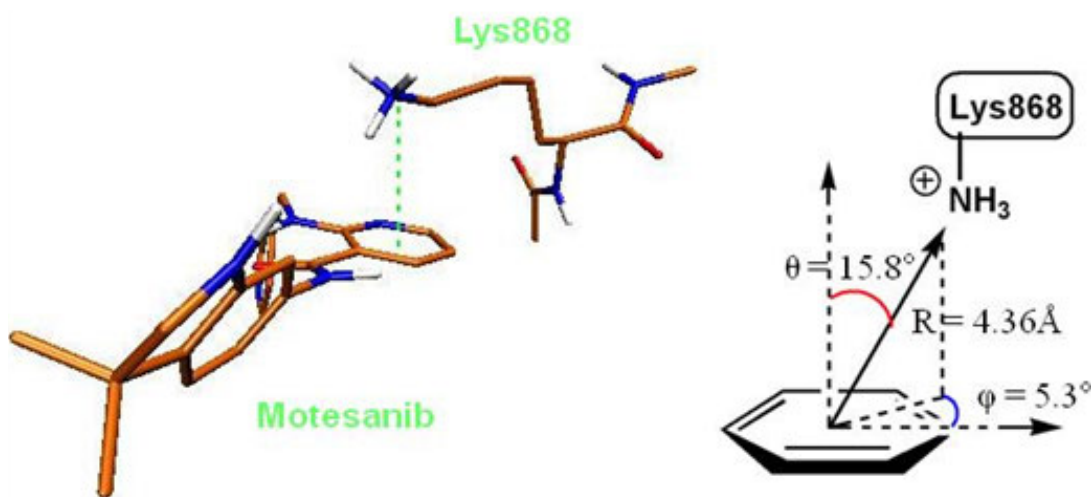


Figure 3. 3D representation of cation- π interaction between Lys868 and Motesanib.

weakens the cation- π binding ability.

The deprotonated Glu885 is the most significant residue for enzyme-inhibitor interactions due to the strong hydrogen bond with the amide NH in AMG 706. Typical charge-assisted hydrogen bond between Glu885 and amide NH was found to be supported by significant binding energy of -26.82 kcal/mol. Another important H-bond between Asp1046 and amide oxygen was associated with -12.96

kcal/mol interaction energy. In the case of Cys919 residue, the observed binding energy was estimated to be -9.06 kcal/mol. In fact hydrogen bonding interaction with Cys919 from H-donor group of the inhibitor is the key feature of VEGFR inhibitors (39).

In ligand-receptor interaction, stereoelectronic effects are prominent in determining complementary potential electrostatic surfaces. Ligand electronic structure may address its proper orientation in the enzyme active site and potent inhibition would be expected regarding proper fitness of the ligand and electronic surfaces of the active site.

Mulliken partial electronic charges were assigned to the constituent atoms of compound AMG 709 (Figure 4) (40). It should be noted that atoms participated in key bindings with Asp1046, Glu885 (charge-assisted interactions) and Cys919 residues possessed relatively negative electronic charges.

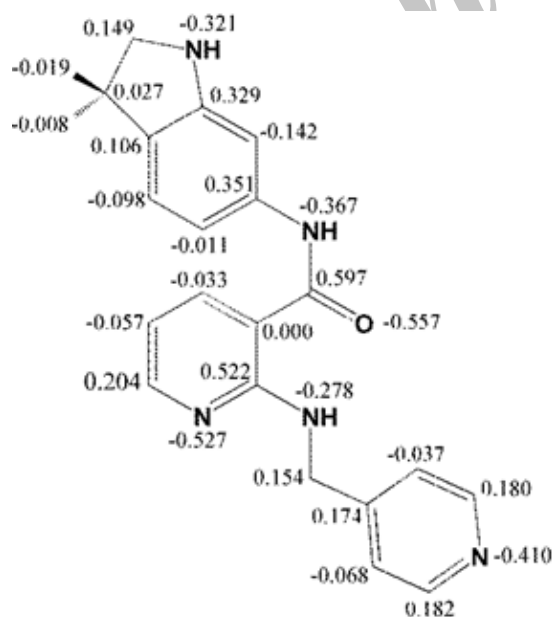


Figure 4. Mulliken partial charge distribution for Motesanib heavy atoms.

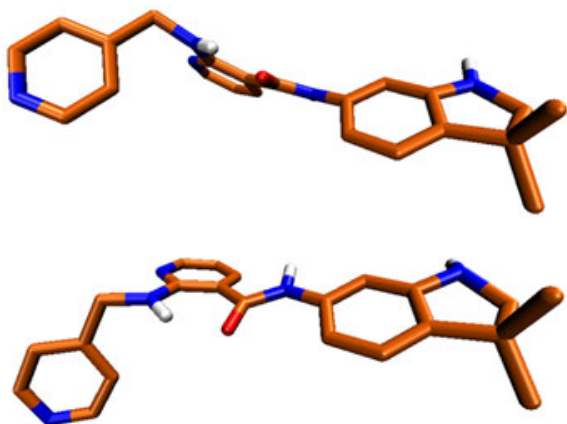


Figure 5. Conformational structure deviation of Motesanib in VEDFR-2 active site (up), and optimized conformer (down).

be defined as an energy difference for ligand in its free and protein bound states within aqueous medium. ΔE_{inst} needs to be considered in order to adjust obtained binding energies. Water was selected as a biological medium for this purpose.

For the purpose of calculating ΔE_{inst} , optimum structural conformation of compound AMG 709 was obtained in water and relevant energy was assigned to the free state. In the next step, the energy of receptor bound ligand was obtained in the crystallographic state. ΔE_{inst} may be well related with the free energy of binding via following equations:

$$\Delta G_b = \Delta H_b - T\Delta S_b \quad \text{Equation (2)}$$

$$\Delta H_b = \Delta E_t - P\Delta V \approx \Delta E_{tb} \quad \text{Equation (3)}$$

$$\Delta E_{tb} = \Delta E_b + \Delta E_{inst} \quad \text{Equation (4)}$$

Higher ΔE_{inst} values support more positive total binding energies (ΔE_{tb}) consequently leading to weaker ligand-receptor interactions in terms of free binding energies (ΔG_b). Our calculations showed that AMG 709 tolerated 8.91 kcal/mol instability to gain the appropriate conformation in binding to the receptor. Based on the obtained results, ΔE_{tb} was found to be -40.36 kcal/mol. Two conformational poses of the ligand are depicted in Figure 5.

However the difference between ΔE_{tb} and ΔG_b values associated with relevant ligand

may account for the participation of solvation in binding profile. In the light of the above information, solvation energy of Motesanib molecule needs must be taken into account for the correlation of ΔE_{tb} and ΔG_b terms. This result might further demonstrate the important role of solvent molecules in determining final free binding energy of ligand-receptor system.

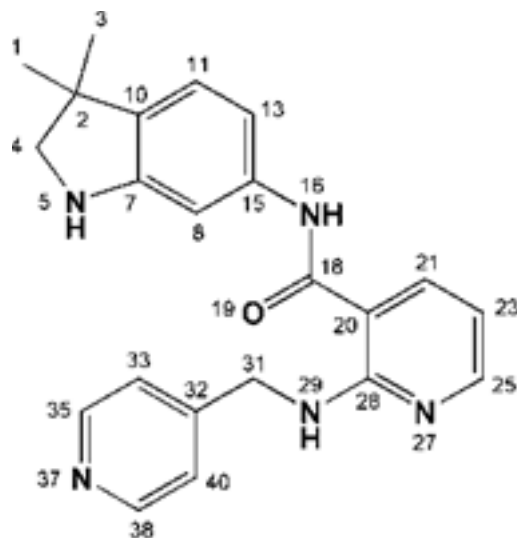
The estimated conformational change of ligand structure upon binding to the receptor was evaluated in a more detailed way via performing comparative conformational analysis of the molecular geometries. For this purpose, optimized 3D structure of AMG 709 was obtained by DFT calculations via B3LYP method in association with split valence basis set using polarization functions (Def2-SVP). Frequency calculation with same basis set was performed to confirm the optimized structure. All frequencies were real and no imaginary frequency was seen. The resulted geometric poses in terms of bond lengths and dihedral angles are summarized in Tables 2 and 3. It should be noticed that due to the uncertainty in the delicate position of hydrogen atoms in crystallographic file, associated data have not been shown in Tables. We found that all the calculated bond lengths of the DFT optimized structure were in adaptable correlation with the crystallographic data.

The varied dihedral angles between optimized and crystallographic ligand poses would be expected upon binding to the receptor active site. AMG 709 adapted some torsional distortions to get proper oriented pharmacophoric points. These well-oriented functional groups might be critical in achieving optimum key interactions with the residues of the VEGFR-2 active site.

Regarding the data in Table 3, some relatively significant angular deviations may be noticed. The observed rotation of C15-C16 bond (Figure 5) let to the noticeable change in C8(13)-C15-N16-C18 dihedral angel (Table 3). This conformational distortion occurred at the amide linker.

All the mentioned conformational changes occurred in the structural moieties participated in interactions with key amino acids of VEGFR-2 active site (Figure 1).

Table 2. Bond lengths of Motesanib in the optimized and crystallographic (VEGFR-2, PDB code: 3EFL) conformers.



Bond	Bond length (Å)		Bond	Bond length (Å)	
	Crystallographic state	Optimized state		Crystallographic state	Optimized state
C1-C2	1.530	1.5453	C18-C20	1.532	1.4925
C1-H42	-	1.0964	O19-H30	-	1.8692
C1-H43	-	1.0946	C20-C21	1.389	1.3977
C1-H44	-	1.0939	C20-C28	1.393	1.4381
C2-C3	1.530	1.5346	C21-H22	-	1.0868
C2-C4	1.528	1.5597	C21-C23	1.391	1.3916
C2-C10	1.530	1.5258	C23-H24	-	1.0837
C3-H45	-	1.0943	C23-C25	1.391	1.3944
C3-H46	-	1.0951	C25-H26	-	1.0892
C3-H47	-	1.0962	C25-N27	1.323	1.3307
C4-N5	1.471	1.4736	N27-C28	1.343	1.3486
C4-H48	-	1.0947	C28-N29	1.332	1.3606
C4-H49	-	1.1017	N29-H30	-	1.016
N5-H6	-	1.0121	N29-C31	1.470	1.446
N5-C7	1.333	1.3981	C31-C32	1.531	1.5218
C7-C8	1.393	1.39	C31-H50	-	1.0978
C7-C10	1.395	1.4056	C31-H51	-	1.0926
C8-H9	-	1.0879	C32-C33	1.392	1.3951
C8-C15	1.393	1.4092	C32-C40	1.392	1.4001
C10-C11	1.392	1.3851	C33-H34	-	1.0848
C11-H12	-	1.087	C33-C35	1.390	1.3966
C11-C13	1.391	1.4021	C35-H36	-	1.0889
C13-H14	-	1.079	C35-N37	1.323	1.3376
C13-C15	1.394	1.4019	N37-C38	1.323	1.3408
C15-N16	1.330	1.4145	C38-H39	-	1.0888
N16-H17	-	1.0084	C38-C40	1.391	1.3922
N16-C18	1.331	1.3731	C40-H41	-	1.0872
C18-O19	1.230	1.2385			

Table 3. Dihedral angles of Motesanib in the optimized and crystallographic (VEGFR-2, PDB code: 3EFL) conformers.

Dihedral angle	Angle (degree)		Dihedral angle	Angle (degree)	
	Crystallographic state	Optimized state		Crystallographic state	Optimized state
H42-C1-C2-C3	-	56.282	C8-C15-N16-C18	-134.086	-178.173
H42-C1-C2-C4	-	-67.538	C13-C15-N16-H17	-	176.423
H42-C1-C2-C10	-	-177.279	C13-C15-N16-C18	52.015	2.511
H43-C1-C2-C3	-	-63.575	C15-N16-C18-O19	1.241	3.4426
H43-C1-C2-C4	-	172.605	C15-N16-C18-C20	-178.813	-177.293
H43-C1-C2-C10	-	62.862	H17-N16-C18-O19	-	-170.398
H44-C1-C2-C3	-	176.567	H17-N16-C18-C20	-	8.8673
H44-C1-C2-C4	-	52.747	N16-C18-C20-C21	15.753	23.472
H44-C1-C2-C10	-	-56.995	N16-C18-C20-C28	-166.812	-158.203
C1-C2-C3-H45	-	178.045	O19-C18-C20-C21	-164.298	-157.260
C1-C2-C3-H46	-	57.839	O19-C18-C20-C28	13.136	21.065
C1-C2-C3-H47	-	-61.358	C18-C20-C21-H22	-	3.080
C4-C2-C3-H45	-	-59.025	C18-C20-C21-C23	177.361	-178.980
C4-C2-C3-H46	-	-179.231	C28-C20-C21-H22	-	-175.305
C4-C2-C3-H47	-	61.572	C28-C20-C21-C23	-0.114	2.635
C10-C2-C3-H45	-	53.925	C18-C20-C28-N27	-177.196	177.765
C10-C2-C3-H46	-	-66.282	C18-C20-C28-N29	2.607	-1.169
C10-C2-C3-H47	-	174.522	C21-C20-C28-N27	0.280	-3.815
C1-C2-C4-N5	-101.759	-88.860	C21-C20-C28-N29	-179.918	177.251
C1-C2-C4-H48	-	31.355	C20-C21-C23-H24	-	-179.516
C1-C2-C4-H49	-	151.806	C20-C21-C23-C25	-0.052	-0.028
C3-C2-C4-N5	133.531	148.232	H22-C21-C23-H24	-	-1.559
C3-C2-C4-H48	-	-91.553	H22-C21-C23-C25	179.979	177.928
C3-C2-C4-H49	-	28.898	C21-C23-C25-H26	-	179.086
C10-C2-C4-N5	15.886	27.029	C21-C23-C25-N27	0.058	-1.787
C10-C2-C4-H48	-	147.243	H24-C23-C25-H26	-	-1.424
C10-C2-C4-H49	-	-92.305	H24-C23-C25-N27	-	177.703
C1-C2-C10-C7	102.711	98.816	C23-C25-N27-C28	0.113	0.682
C1-C2-C10-C11	-74.692	-78.169	H26-C25-N27-C28	-	179.846
C3-C2-C10-C7	-133.134	-136.914	C25-N27-C28-C20	-0.285	2.216
C3-C2-C10-C11	49.463	46.101	C25-N27-C28-N29	179.914	-178.813
C4-C2-C10-C7	-15.307	-17.309	C20-C28-N29-H30	-	-8.165
C4-C2-C10-C11	167.290	165.705	C20-C28-N29-C31	171.865	-177.332
C2-C4-N5-H6	-	-161.533	N27-C28-N29-H30	-	172.857
C2-C4-N5-C7	-12.375	-28.598	N27-C28-N29-C31	-8.334	3.690
H48-C4-N5-H6	-	77.305	C28-N29-C31-C32	94.086	102.346
H48-C4-N5-C7	-	-149.760	C28-N29-C31-H50	-	-135.519
H49-C4-N5-C6	-	-43.223	C28-N29-C31-H51	-	-19.574
H49-C4-N5-C7	-	89.712	H30-N29-C31-C32	-	-66.239
C4-N5-C7-C8	-170.367	-163.627	H30-N29-C31-H50	-	55.896
C4-N5-C7-C10	2.573	18.132	H30-N29-C31-H51	-	171.841
H6-N5-C7-C8	-	-31.016	N29-C31-C32-C33	5.187	-4.398
H6-N5-C7-C10	-	150.744	N29-C31-C32-C40	-173.633	175.611

Table 3. (Continue).

Dihedral angle	Angle (degree)		Dihedral angle	Angle (degree)	
	Crystallographic state	Optimized state		Crystallographic state	Optimized state
N5-C7-C8-H9	-	2.343	H50-C31-C32-C33	-	-126.654
N5-C7-C8-C15	171.649	-177.916	H50-C31-C32-C40	-	53.354
C10-C7-C8-H9	-	-179.584	H51-C31-C32-C33	-	116.660
C10-C7-C8-C15	-0.751	0.156	H51-C31-C32-C40	-	-63.331
N5-C7-C10-C2	8.568	0.493	C31-C32-C33-H34	-	0.520
N5-C7-C10-C11	-173.683	177.903	C31-C32-C33-C35	-178.533	-179.807
C8-C7-C10-C2	-177.684	-177.894	C40-C32-C33-H34	-	-179.489
C8-C7-C10-C11	0.066	-0.484	C40-C32-C33-C35	0.297	0.184
C7-C8-C15-C13	1.044	-0.027	C31-C32-C40-C38	178.603	179.705
C7-C8-C15-N16	-172.919	-179.364	C31-C32-C40-H41	-	-0.199
H9-C8-C15-C13	-	179.715	C33-C32-C40-C38	-0.223	-0.288
H9-C8-C15-N16	-	0.378	C33-C32-C40-H41	-	179.809
C2-C10-C11-H12	-	-3.188	C32-C33-C35-H36	-	-179.948
C2-C10-C11-C13	177.471	177.413	C32-C33-C35-N37	-0.201	0.009
C7-C10-C11-H12	-	-179.917	H34-C33-C35-H36	-	-0.274
C7-C10-C11-C13	0.316	0.684	H34-C33-C35-N37	-	179.683
C10-C11-C13-H14	-	179.731	C33-C35-N37-C38	0.036	-0.095
C10-C11-C13-C15	-0.019	-0.558	H36-C35-N37-C38	-	179.863
H12-C11-C13-H14	-	0.323	C35-N37-C38-H39	-	-179.957
H12-C11-C13-C15	-	-179.966	C35-N37-C38-C40	0.031	-0.018
C11-C13-C15-C8	-0.654	0.224	N37-C38-C40-C32	0.070	0.214
C11-C13-C15-N16	173.284	179.508	N37-C38-C40-H41	-	-179.882
H14-C13-C15-C8	-	179.938	H39-C38-C40-C32	-	-179.849
H14-C13-C15-N16	-	-0.777	H39-C38-C40-H41	-	0.055
C8-C15-N16-H17	-	-4.261			

Conclusion

Amino acid decomposition analysis provided further insight into the effect of individual amino acid residues on Motesanib/VEGFR-2 binding profile. Such structure-based studies may serve as efficient analyzing tools in evaluating the pharmacophore models. Owing to the prominent role of electrostatic forces in initial ligand-receptor interactions, charge-assisted H-bonds and cation- π interactions need to be particularly attended. In the case of Cys919, the estimated binding energy could further confirm the role of this key amino acid in contribution to H-bond interactions reported for various VEGFR inhibitors. We could further demonstrate that Motesanib does not necessarily bind to the receptor in its optimum conformation state.

Acknowledgements

Financial supports of this project by research council of Shiraz University of Medical Sciences are acknowledged.

References

- (1) Rapisarda A and Melillo G. Role of the VEGF/VEGFR axis in cancer biology and therapy. *Adv. Cancer Res.* (2012) 114: 237-267.
- (2) Hicklin DJ and Ellis LM. Role of the vascular endothelial growth factor pathway in tumor growth and angiogenesis. *J. Clin. Oncol.* (2005) 23: 1011-1027.
- (3) Ferrara N, Gerber HP and LeCouter J. The biology of VEGF and its receptors. *Nat. med.* (2003) 9: 669-676.
- (4) Strawn LM, McMahon G, App H, Schreck R, Kuchler WR, Longhi MP, Hui TH, Tang C, Levitzki A and Gazit A. Flk-1 as a target for tumor growth inhibition. *Cancer Res.* (1996) 56: 3540-3545.

- (5) Silva SR, Bowen KA, Rychahou PG, Jackson LN, Weiss HL, Lee EY, Townsend Jr CM and Evers BM. VEGFR 2 expression in carcinoid cancer cells and its role in tumor growth and metastasis. *Int. J. CANCER*. (2011) 128: 1045-1056.
- (6) Hanahan D and Folkman J. Patterns and emerging mechanisms of the angiogenic switch during tumorigenesis. *Cell*. (1996) 86: 353-364.
- (7) Dvorak HF. Vascular permeability factor/vascular endothelial growth factor: a critical cytokine in tumor angiogenesis and a potential target for diagnosis and therapy. *J. Clin. Oncol.* (2002) 20: 4368-4380.
- (8) Carmeliet P. Angiogenesis in life, disease and medicine. *Nature* (2005) 438: 932-936.
- (9) Ferrara N and Gerber HP. The role of vascular endothelial growth factor in angiogenesis. *Acta. Haematol-Basel.* (2000) 106: 148-156.
- (10) Peruzzi B and Bottaro DP. Targeting the c-Met signaling pathway in cancer. *Clin. Cancer Res.* (2006) 12: 3657-3657.
- (11) Ferrara N. Vascular endothelial growth factor as a target for anticancer therapy. *Oncologist.* (2004) 9: 2-10.
- (12) Holmes K, Roberts OL, Thomas AM and Cross MJ. Vascular endothelial growth factor receptor-2: structure, function, intracellular signalling and therapeutic inhibition. *Cell. Signalling.* (2007) 19: 2003-2012.
- (13) Sun L, Tran N, Liang C, Hubbard S, Tang F, Lipson K, Schreck R, Zhou Y, McMahon G and Tang C. Identification of Substituted 3-[(4,5,6,7-Tetrahydro-1H-indol-2-yl)methylene]-1,3-dihydroindol-2-ones as Growth Factor Receptor Inhibitors for VEGF-R2 (Flk-1/KDR), FGF-R1, and PDGF-R β Tyrosine Kinases. *J. Med. Chem.* (2000) 43: 2655-2663.
- (14) Bold G, Altmann KH, Frei J, Lang M, Manley PW, Traxler P, Wietfeld B, Bruggen J, Buchdunger E, Cozens R, Ferrari S, Furet P, Hofmann F, Artinybaron G, Mestan J, Rosel J, Sills M, Stover D, Acemoglu F, Boss E, Emmenegger R, Lasser L, Masso E, Roth R, Schlachter C and Vetterli W. New anilinothalazines as potent and orally well absorbed inhibitors of the VEGF receptor tyrosine kinases useful as antagonists of tumor-driven angiogenesis. *J. Med. Chem.* (2000) 43: 2310-2323.
- (15) Hennequin LF, Stokes ES, Thomas AP, Johnstone C, Plé PA, Ogilvie DJ, Dukes M, Wedge SR, Kendrew J and Curwen JO. Novel 4-Anilinoquinazolines with C-7 Basic Side Chains: Design and Structure Activity Relationship of a Series of Potent, Orally Active, VEGF Receptor Tyrosine Kinase Inhibitors. *J. Med. Chem.* (2002) 45: 1300-1312.
- (16) Bilodeau MT, Rodman LD, McGaughey GB, Coll KE, Koester TJ, Hoffman WF, Hungate RW, Kendall RL, McFall RC, Rickert KW, Rutledge RZ and Thomas KA. The discovery of N-(1,3-thiazol-2-yl)pyridin-2-amines as potent inhibitors of KDR kinase. *Bioorg. Med. Chem. Lett.* (2004) 14: 2941-2945.
- (17) Bilodeau MT, Cunningham AM, Koester TJ, Ciecko PA, Coll KE, Huckle WR, Hungate RW, Kendall RL, McFall RC, Mao X, Rutledge RZ and Thomas KA. Synthesis and inhibitory activity of ubiquinone-acetogenin hybrid inhibitor with bovine mitochondrial complex I. *Bioorg. Med. Chem. Lett.* (2003) 13: 2385-2388.
- (18) Wu Z, Fraley ME, Bilodeau MT, Kaufman ML, Tasber ES, Balitza AE, Hartman GD, Coll KE, Rickert K, Shipman J, Shi B, Sepp-Lorenzino L and Thomas KA. Design and synthesis of 3,7-diarylimidazopyridines as inhibitors of the VEGF-receptor KDR. *Bioorg. Med. Chem. Lett.* (2004) 14: 909-912.
- (19) Fraley ME, Arrington KL, Buser CA, Ciecko PA, Coll KE, Fernandes C, Hartman GD, Hoffman WF, Lynch JJ, McFall RC, Rickert K, Singh R, Smith S, Thomas KA and Wong BK. Optimization of the indolyl quinolinone class of KDR (VEGFR-2) kinase inhibitors: effects of 5-amido- and 5-sulphonamido-indolyl groups on pharmacokinetics and hERG binding. *Bioorg. Med. Chem. Lett.* (2004) 14: 351-355.
- (20) Anderson AC. Structure-based functional design of drugs: from target to lead compound. *Method. Mol. Biol.* (2012) 823: 359-366.
- (21) Bohacek RS, McMartin C and C GW. The art and practice of structure-based drug design: A molecular modeling perspective. *Med. Res. Rev.* (1996) 16: 3-50.
- (22) Sherman SI, Wirth LJ, Droz JP, Hofmann M, Bastholt L, Martins RG, Licitra L, Eschenberg MJ, Sun YN and Juan T. Motesanib diphosphate in progressive differentiated thyroid cancer. *N. Engl. J. Med.* (2008) 359: 31-42.
- (23) Rosen LS, Kurzrock R, Mulay M, Vugt AV, Purdom M, Ng C, Silverman J, Koutsoukos A, Sun Y-N, Bass MB, Xu RY, Polverino A, Wizeorek JS, Chang DD, Benjamin R and S HR. Safety, pharmacokinetics, and efficacy of AMG 706, an oral multikinase inhibitor, in patients with advanced solid tumors. *J. Clin. Oncol.* (2007) 25: 2369-2376.
- (24) Coxon A, Bush T, Saffran T, Kaufman S, Belmontes B, Rex K, Hughes P, Caenepeel S, Rottman JB, Tasker A, Patel V, Kendall R, Radinsky R and Polverino A. Broad antitumor activity in breast cancer xenografts by motesanib, a highly selective, oral inhibitor of vascular endothelial growth factor, platelet-derived growth factor, and kit receptors. *Clin. Cancer Res.* (2009) 15: 110-118.
- (25) Sherman SI, Wirth LJ, Droz J-P, Hofmann M, Bastholt L, Martins RG, Licitra L, Eschenberg MJ, Sun Y-N, Juan T, Stepan DE and Schlumberger MJ. Motesanib diphosphate in progressive differentiated thyroid cancer. *N. Engl. J. Med.* (2008) 359: 31-42.
- (26) Razzaghi-Asl N, Ebadi A, Edraki N, Shahabipour S and Miri R. Fragment-based Binding Efficiency Indices in Bioactive Molecular Design: A Computational Approach to BACE-1 Inhibitors. *Iran. J. Pharm. Res.* (2013) 12: 423-436.
- (27) Vedani A, Zbinden P, Snyder JP and Greenidge PA. Pseudoreceptor Modeling: The Construction of Three-Dimensional Receptor Surrogates. *J. Am. Chem. Soc.* (1995) 117: 4987-4994

- (28) Bissantz C, Folkers G and Rognan D. Protein-Based Virtual Screening of Chemical Databases. 1. Evaluation of Different Docking/Scoring Combinations. *J. Med. Chem.* (2000) 43: 4759-4767.
- (29) Kubinyi H. QSAR and 3D QSAR in drug design Part 1: methodology. *Drug Discov. Today.* (1997) 2: 457-467.
- (30) Neese F ORCA – an ab initio, Density Functional and Semiempirical program package, Version 2.8.0 University of Bonn (2011).
- (31) Remko M, Boháč A and Kovačikova L. Molecular structure, pKa, lipophilicity, solubility, absorption, polar surface area, and blood brain barrier penetration of some antiangiogenic agents. *Struct. Chem.* (2011) 22: 635-648.
- (32) Miri R, Firuzi O, Peymani P, Nazarian Z and Shafiee A. Synthesis and cytotoxicity study of new cyclopenta [b] quinoline-1, 8-dione derivatives. *Iran. Pharm. J. Res.* (2011) 3: 489-496.
- (33) Schaefer A, Horn H and Ahlrichs R. Property-optimized Gaussian basis sets for molecular response calculations. *J. Chem. Phys.* (1992) 97: 2571-2582.
- (34) Wang Z, Canagarajah BJ, Boehm JC, Kassis S, Cobb MH, Young PR, Abdel-Meguid S, Adams JL and Goldsmith EJ. Structural basis of inhibitor selectivity in MAP kinases. *Structure.* (1998) 6: 1117-1128.
- (35) Humphrey W, Dalke A and Schulten K. VMD: visual molecular dynamics. *J. Mol. Graphics.* (1996) 14: 33-38.
- (36) Levine IN (2008) Physical chemistry. McGraw-Hill, Dougherty DA. Cation- π Interactions in Chemistry and Biology: A New View of Benzene, Phe, Tyr, and Trp. *Sci.* (1996) 271: 163-168.
- (37) Ma JC and Dougherty DA. The cation- π interaction. *Chem. Rev.* (1997) 97: 1303-1324.
- (38) Gallivan JP and Dougherty DA. A Computational Study of Cation- π Interactions vs. Salt Bridges in Aqueous Media: Implications for Protein Engineering. *J. Am. Chem. Soc.* (2000) 122: 870-874.
- (39) Gill AL, Verdonk M, Boyle RG and Taylor R. A comparison of physicochemical property profiles of marketed oral drugs and orally bioavailable anti-cancer protein kinase inhibitors in clinical development. *Curr. Top. Med. Chem.* (2007) 7: 1408-1422.
- (40) Mulliken R. Electronic Population Analysis on LCAO MO Molecular Wave Functions. IV. Bonding and Antibonding in LCAO and Valence Bond Theories. *J. Chem. Phys.* (1955) 23: 2343-2346.

This article is available online at <http://www.ijpr.ir>
